IEEE Access
Multidisciplinary | Rapid Review | Open Access Journal

Received August 20, 2019, accepted September 1, 2019, date of publication September 5, 2019,
date of current version September 20, 2019.

Digital Object Identifier 10.1109/ACCESS.2019.2939640

Image Registration Based on Camera Calibration for Dual-Wavelength Retinal Oximetry

YONG-LI XIAN[1], CONG-ZHENG WANG[2], AND YUN DAI[3]
[1]School of Electrical Engineering and Electronic Information, Xihua University, Chengdu 610039, China
[2]Institute of Optics and Electronics, Chinese Academy of Sciences, Chengdu 610209, China
[3]The Laboratory on Adaptive Optics, Institute of Optics and Electronics, Chinese Academy of Sciences, Chengdu 610209, China

Corresponding author: Yong-Li Xian (xyl123@mail.ustc.edu.cn)

This work was supported by the National Science Foundation of China under Grant 61805248.

ABSTRACT Retinal images at 570nm and 600nm are simultaneously captured by retinal oximetry. However, there exists misalignment between the two images, which should be adjusted before they are used to analyze hemoglobin oxygen saturation (SO_2). Having a robust, accurate and fast registration scheme can ensure accuracy and speed of SO_2 calculation. However, the existing retinal image registration methods cannot meet demand for clinical application of retinal oximetry. For example, errors in the vessel segmentation from each image cause corresponding errors in the registration, point matches may become unreliable when the predefined matching cost is corrupted by pathological retinal images. And it is always a time-consuming task. In this paper, we first analyzed the misalignment reason between dual-wavelength images, and concluded that there only exists the rotation and translation deviation between the two images caused by a mounting deviation of CCD cameras. The parameters were only related to system itself. Based on this, we proposed a registration method based on camera calibration that benefits from feature extraction and affine transformation matrix calculation. The parameters obtained by the proposed method were tested on 80 pairs of retinal images of 5 healthy volunteers and the results showed that the proposed method can successfully register the dual-wavelength images. The proposed registration method can significantly improve SO_2 calculation speed while ensuring accuracy.

INDEX TERMS Retinal oximetry, SO_2, image registration, camera calibration.

I. INTRODUCTION

The SO_2 in retinal vessels can provide doctors with important clinical information about the metabolic state of the retina [1]. For example, assessment of SO_2 in the optic nerve head may help early diagnosis of glaucoma and is crucial for timely effective treatment [2]. Monitoring SO_2 changes in retina could evaluate relationships between oxygen consumption, blood sugar levels, and vascular function in diabetic retinopathy [3]. Therefore, from the clinical prospective, retinal oximetry can directly provide clinicians with an insight into structures and function they need to follow/monitor for diagnosis or management.

Among numerous SO_2 measurement techniques in retinal vessels, dual-wavelength retinal oximetry based on fundus camera has been proved effective [4]. It is based on the different optical properties of oxygenated hemoglobin (HbO_2) and hemoglobin (Hb). Several versions of the oximeters, which are based on the same principle, have been reviewed in literature [5]. The system simultaneously collects images at two wavelengths: one is sensitive to changes of HbO_2 in the blood and the other is an isosbestic wavelength for HbO_2 and Hb. The SO_2 values in the retinal vessels are finally measured after vessel segmentation, image registration and calculation of optic density ratio of two images. Fig. 1 shows two retinal images of human eye with 45 deg. view field acquired simultaneously at 570nm and 600nm. The 570nm image, which

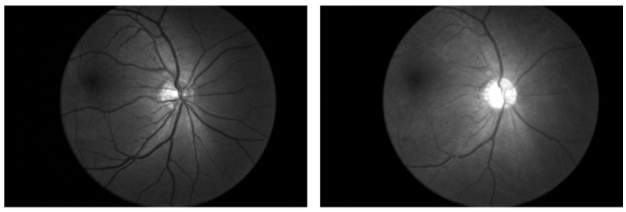

FIGURE 1. Dual-wavelength fundus images: (a) retinal image at 570nm (b) retinal image at 600nm.

The associate editor coordinating the review of this manuscript and approving it for publication was Mahmoud Al Ahmad.

is insensitive to HbO_2 change, has higher contrast between the blood vessels and the background than does the image at 600 nm.

However, there exists misalignment between dual-wavelength images, which should be adjusted before the calculation of SO_2. Having a robust, accurate and fast registration scheme can ensure accuracy and speed of SO_2 calculation. Although image registration, especially retinal image registration, is well known in the literature [6]–[12], there has been very little work on the study of spectrophotometric image registration. Halldorsson proposed a retinal image registration algorithm which was a more data-oriented method and could complete four wavelength images registration at very low resolution [13]. In an earlier paper, employing a hybrid registration algorithm based on vessel segmentation and optic disc location, we demonstrated that the proposed method can realize registration [14]. Theoretically speaking, most of the existing retinal image registration techniques, which can be divided into feature-based, gray-information-based, and hybrid methods, can be used for estimating and eliminating the spatial misalignment between dual-wavelength images with certain adaptions. However, they are limited according to our experiments because of several basic reasons. First, feature-based methods can realize the registration for local feature, but they have their drawbacks in certain conditions. For example, point matches may become unreliable when the predefined matching cost is corrupted by the anatomic/metabolic variations of retina across images [15]–[18]. And many existing retinal images registration approaches contain a vessel segmentation step, as the retinal blood vessels are the most dominant structures that are in common between the pair of images. However, errors in the vessel segmentation from each image may cause corresponding errors in the registration, especially for unhealthy retinal images [19]–[23]. This cannot meet the requirement of high precision for SO_2 measurement in the retinal oximetry. Second, gray-information-based methods which can directly use all available grayscale information [24]–[26], can improve registration accuracy and robustness, but it is a time-consuming task, and also not suitable for clinical application of retinal oximetry. Hence, retinal image registration methods which have been proposed earlier did not seem to solve the aforementioned problem.

In order to reduce registration time and improve registration accuracy, we first analyzed in detail the reason for misalignment between dual-wavelength images, and concluded that there only exists the rotation and translation deviation between the two images of 570 nm and 600 nm caused by a mounting deviation of CCD cameras. The registration parameters were only related to system itself. Therefore, the corresponding parameters are fixed under the condition of no external force. For example, they do not vary from person to person, and do not change with the time, angle of gaze, and so on. Hence, we proposed a registration method based on camera calibration that benefits from feature extraction and affine transformation matrix calculation. The parameters obtained by the proposed method were tested on 80 pairs of retinal images of 5 healthy volunteers and the results showed that the proposed method can successfully register the multimodal images. The total process is simple, convenient, and efficient for retinal oximetry. Once the affine translation parameters are determined, they can be written into the retinal oxygen saturation calculation software. The misalignment can be automatically eliminated after inputting the dual-wavelength retinal image. It does not need subsequent dual-wavelength retinal image registration every time.

The paper is organized as follows. Section II describes the system and reason analysis for misalignment between dual-wavelength images. Section III presents experiment procedures. Section IV presents the experimental results and evaluation. Finally, discussions and conclusions are drawn in section V and section VI, respectively.

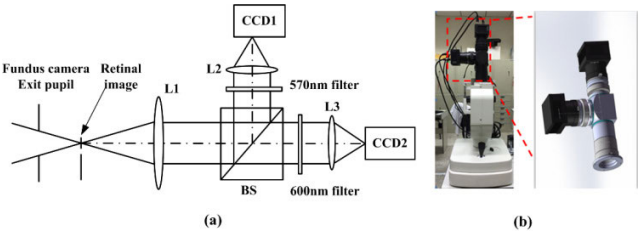

FIGURE 2. (a)Schematic of the dual-wavelength retinal image acquisition subsystem;(b)Picture of dual-wavelength retinal image acquisition subsystem.

II. SYSTEM

In this paper, we use the same dual-wavelength image acquisition system developed by our lab [27]. The optical path of the dual-wavelength retinal image acquisition system can be seen in Fig.2 (a). The outputs of the CCDs are sent to a computer where the dual-wavelength images are stored. Fig.2 (b) is the picture of dual-wavelength retinal image acquisition system.

A. REASON ANALYSIS FOR MISALIGNMENT BETWEEN DUAL-WAVELENGTH IMAGES

From the schematic of the dual-wavelength retinal imaging system, the output retinal image of the fundus camera is separated by a 5:5 beam splitter (50% transmission and 50% reflection) into two parts, and finally simultaneously reimaged on the two CCDs. Additionally, there is nearly no distortion in the dual-wavelength retinal images because of the design of optical system and light path adjustment. Hence, there only exists the rotation and translation deviation between the two images of 570 nm and 600 nm caused by a mounting deviation of CCD cameras. It should be adjusted before the calculation of SO_2. And the parameters do not change with external conditions, for example, they do not vary from person to person, and do not change with the time. They are only related to the system itself. The image rotation and translation can affect the subsequent image processing and lead to substantial uncertainties in the

calculated SO_2. Therefore, we proposed a robust registration framework based on camera calibration, it is capable of aligning dual-wavelength images without requiring retinal image registration every time with the aim of speeding up the registration process and improving registration accuracy. To our knowledge, such studies in the image registration based on camera calibration in the retinal oximetry have not yet been reported.

III. EXPERIMENT PROCEDURES

The whole experiment includes two parts: the first part is parameters measurement based on camera calibration; the second part is image registration for dual-wavelength retinal images using the obtained parameters.

A. CALIBRATION PLATE IMAGES ACQUISITION

For the experiment with camera calibration, a set of image pairs for calibration plate acquired by the dual-wavelength image acquisition system are utilized. The calibration target is a dot calibration plate with 9 × 9 corner points evenly distributed and the distance between the adjacent points is 1.0 mm in the horizontal and the vertical directions. The calibration plate was fixed on a mounting bracket and was placed at the position of retinal image in Fig. 2. A series of 20 pairs of images are acquired at different positions by two CCDs simultaneously.

TABLE 1. Location scenario for calibration plate.

Scenario	Translation/mm	Rotation/degrees
1	5(up)	0
2	5(down)	0
3	5(left)	0
4	5(right)	0
5	0	0(clockwise)
6	0	90(clockwise)
7	0	180(clockwise)
8	0	270(clockwise)
9	5(up)	90(clockwise)
10	5(up)	180(clockwise)
11	5(up)	270(clockwise)
12	5(down)	90(clockwise)
13	5(down)	180(clockwise)
14	5(down)	270(clockwise)
15	5(right)	90(clockwise)
16	5(right)	180(clockwise)
17	5(right)	270(clockwise)
18	5(left)	90(clockwise)
19	5(left)	180(clockwise)
20	5(left)	270(clockwise)

In our setting, 20 typical experimental conditions for standard calibration plate are provided in Table 1. A sample of image pairs can be seen in Fig. 3.

B. PARAMETERS MEASUREMENT BASED ON CAMERA CALIBRATION

This procedure mainly includes image processing for calibration plate and matrix acquisition for affine transformation.

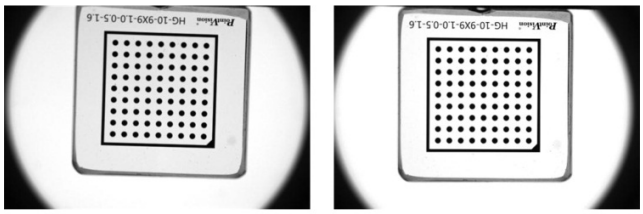

FIGURE 3. A sample of image pairs used for registration: (a) 570 nm image; (b) 600nm image.

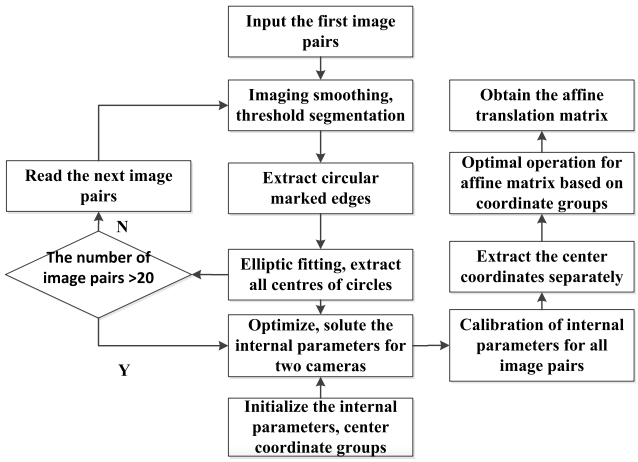

FIGURE 4. The block diagram of image registration based on camera calibration.

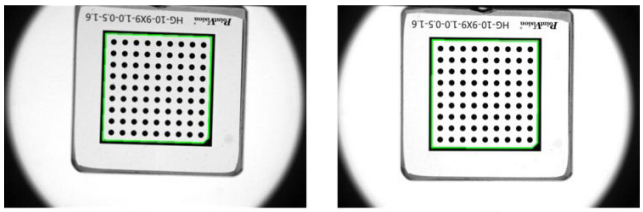

FIGURE 5. The rectangular box for the calibration plate images: (a) 570 nm image; (b) 600nm image.

The algorithm for the whole procedure is based on the famous machine vision software – Halcon [28], which is always employed in the precision measurement of binocular vision system [29], [30]. And the block diagram can be seen in Fig.4.

The specific steps are as follows:

(1) The calibration plate is pasted on a flat bracket and moved into the camera field of view.

(2) The calibration plate is adjusted to take 20 pairs of images at different position according to Table 1, an image pair is shown in Fig.3.

(3) The captured image pairs are processed in turn, including image smoothing, threshold segmentation, and finally the rectangular box of the calibration plate is extracted, corresponding results for Fig. 3 can be seen in Fig. 5.

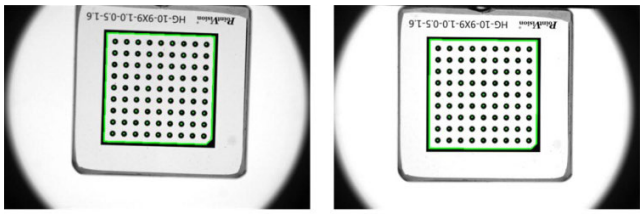

FIGURE 6. The marking point of the calibration plate images: (a) 570 nm image; (b) 600nm image.

(4) In the rectangular box, the edges of all the circular marks are obtained based on the canny operator, and the centre coordinates of all mark points are obtained based on the edge elliptic fitting, corresponding results for Fig. 3 can be seen in Fig. 6. The detection accuracy for edge and centre coordinates can achieve sub-pixel level.

(5) When the centre coordinates of all image pairs are obtained, the camera internal parameters are calculated based on the nonlinear optimization of the centre coordinate group, according to the initial internal parameters.

(6) Based on the camera internal parameters, all images distortion can be corrected in turn, and the centre coordinates of the mark points are re-extracted for each image.

(7) Based on the corrected coordinate group, the corresponding affine transformation matrices for 20 pairs of images are calculated in turn, according to the equation (1)-(2), calculate affine transformation matrix HomMat2D [29].

$$\sum_i \left\| \begin{bmatrix} \mathrm{Qx}[i] \\ \mathrm{Qy}[i] \\ 1 \end{bmatrix} - \mathrm{HomMat2}D * \begin{bmatrix} \mathrm{Px}[i] \\ \mathrm{Py}[i] \\ 1 \end{bmatrix} \right\|^2 = \min \quad (1)$$

where Qx[i] and Qy[i] are horizontal and vertical coordinate values of the i-th characteristic point in the 570nm image, respectively. And Px[i] and Py[i] are horizontal and vertical coordinate values of the i-th characteristic point in the 600nm image, respectively.

$$\begin{aligned} \mathrm{HomMat2}D &= \begin{bmatrix} 1 & 0 & Tx \\ 0 & 1 & Ty \\ 0 & 0 & 1 \end{bmatrix} * \begin{bmatrix} \cos(Phi) & -\sin(Phi) & 0 \\ \sin(Phi) & \cos(Phi) & 0 \\ 0 & 0 & 1 \end{bmatrix} \\ &* \begin{bmatrix} \cos(\mathrm{Th}X) & 0 & 0 \\ \sin(\mathrm{Th}X) & 1 & 0 \\ 0 & 0 & 1 \end{bmatrix} \\ &* \begin{bmatrix} 1 & -\sin(ThY) & 0 \\ 0 & \cos(ThY) & 0 \\ 0 & 0 & 1 \end{bmatrix} * \begin{bmatrix} Sx & 0 & 0 \\ 0 & Sy & 0 \\ 0 & 0 & 1 \end{bmatrix} \end{aligned} \quad (2)$$

where Tx and Ty are horizontal and vertical direction translation, respectively. Phi is rotation angle. ThX and ThY are horizontal and vertical directional tilt angle, respectively. And Sx and Sy are horizontal and vertical directional zoom factor, respectively.

(8) 20 groups of matrices are averaged to obtain the most optimal affine transformation matrix. Now, the accuracy of Tx and Ty in the affine transformation matrix can achieve sub-pixel level.

C. DUAL-WAVELENGTH RETINAL IMAGES ACQUISITION

In order to verify our conclusion, the parameters obtained by the proposed method were tested on 80 pairs of retinal images of 5 healthy volunteers aged between 25 and 30, including their right eyes and left eyes. Paralysis of accommodation and dilation of pupil was achieved through administering 1% cyclopentolate. Informed consent was obtained from all subjects and the experiment procedures conformed to the tenets of the Declaration of Helsinki. Some of those dual-wavelength retinal images were taken at the same day, while others were taken at the different day. To evaluate the effect of the angle of gaze on parameters measurements, retinal image for the same eye was acquired four times. The four typical experimental conditions can be shown in Table 2. That is, location of the same optics disc was changed with gaze. For each volunteers, the measurement was operated only once for all scenarios except scenario 2. The measurements were repeated 5 times for scenario 2 in order to evaluate the effect of the proposed registration method on the reproducibility of the retinal oximetry. Dual-wavelength retinal images for the 4 experimental conditions with one subject can be seen in Fig. 7.

TABLE 2. Scenario for angle of gaze of the same eye.

Scenario	Angle of gaze
1	images centered on the macula
2	images centered on the optic disc
3	images where the subject looked up
4	images where the subject looked down

D. CALIBRATION TARGET IMAGES AND RETINAL IMAGES ACQUISITION THROUGH RE-MOUNTING CCD CAMERAS

In order to discuss about how re-mounting CCD cameras can affect the affine transformation matrix parameters, we re-mounted CCD cameras 2 times. And the calibration target images and dual-wavelength images were acquired according to the aforementioned steps.

IV. EXPERIMENTAL RESULTS AND EVALUATION

A. AFFINE TRANSFORMATION MATRIX PARAMETERS RESULITS

In order to evaluate the stability of the affine transformation matrix, we plotted the matrix parameters based on the 20 pairs of calibration plate images under the conditions of two mounting results. For each mounting, they include two directional translational parameters, and rotation value, two directional tilt angle, and two directional zoom factors, respectively, as shown in Fig. 8 and Fig. 9. Fig.8 represents the first mounting results, and Fig.9 represents the second

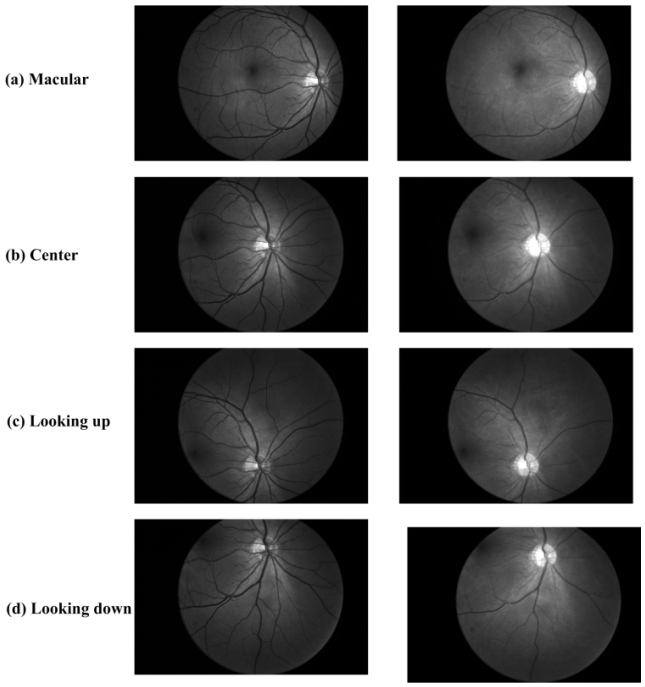

FIGURE 7. Dual-wavelength retinal images for the 4 experimental conditions with the subjects. First, a fundus image centered on the macula was obtained (a), then an image centered on the optic disc (b), followed by images where the subject looked up (c), then down (d).

mounting results. The mean and standard deviation can be also seen in Fig. 8 and Fig.9. For Fig.8, the maximum deviation for right translation is less than 0.3263 pixels, the maximum deviation for up translation is less than 0.4023 pixels, the maximum deviation for rotation is less than 0.0340 degree. For Fig.9, the maximum deviation for right translation is less than 0.4272 pixels, the maximum deviation for up translation is less than 0.3834 pixels, the maximum deviation for rotation is less than 0.0390 degree. It is worth noting that both ThX and ThY (tilt angle for horizontal direction and vertical direction) are equal to 0, both Sx and Sy (zoom factors for horizontal direction and vertical direction) approximately equal to 1 in both Fig.8 and Fig.9. It agrees well with our system design. The mean and standard deviation (Std) for the affine transformation parameters show that our proposed method can achieve sub-pixel accuracy. And it indicated that affine transformation matrix for each mounting has high stability, and can be directly applied in the retinal oximetry. The following experimental results were based on the first affine transformation matrix.

According to above analysis, once the CCD cameras were mounted well, the image pairs for calibration plate can be corrected separately based on the calibrated parameters. If directly overlaying the two images in Fig. 3 without image registration, we can find there obviously exits misalignment between the two images, as can be shown in Fig. 10(a). By using the final affine transformation matrix to transform one image, and the fusion image is shown in Fig. 10(b), and the validity of the registration can be obtained from the image.

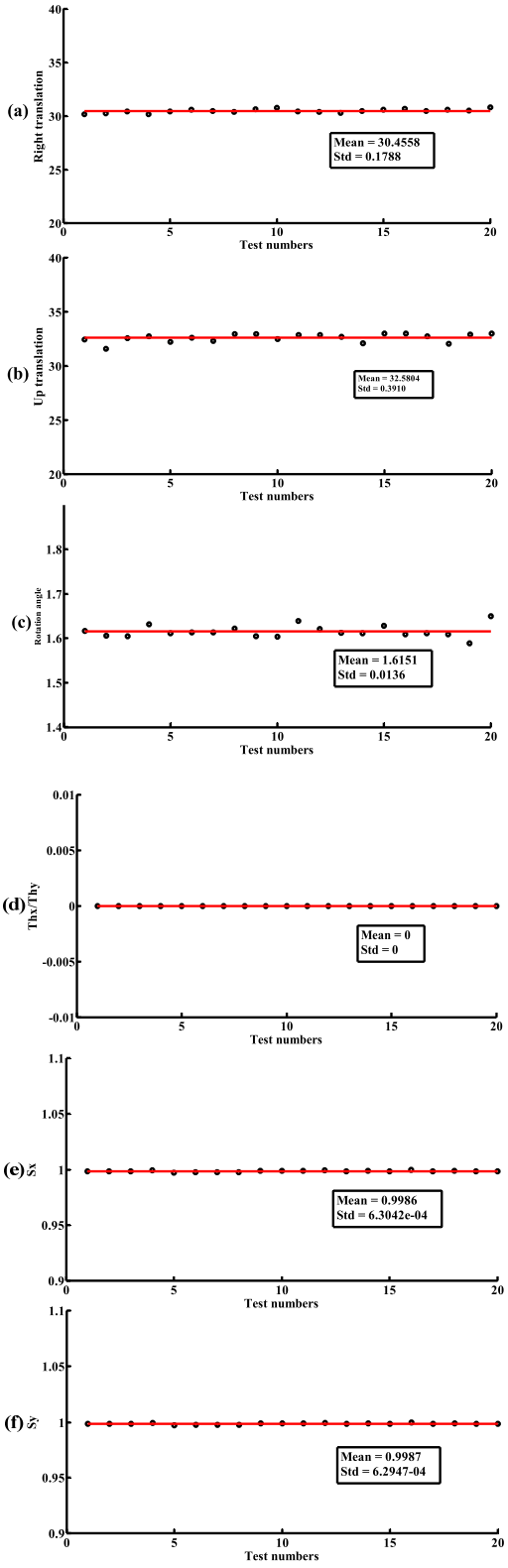

FIGURE 8. Affine transformation matrix parameters for 20 pairs calibration plate images: (a) translation pixels for horizontal direction; (b) translation pixels for vertical direction; (c) rotation angle; (d) tilt angle ThX and ThY for horizontal and vertical direction; (e) zoom factor for horizontal direction Sx; (f) zoom factor for vertical direction Sy. All parameters were measured under the condition of 570nm image as a benchmark.

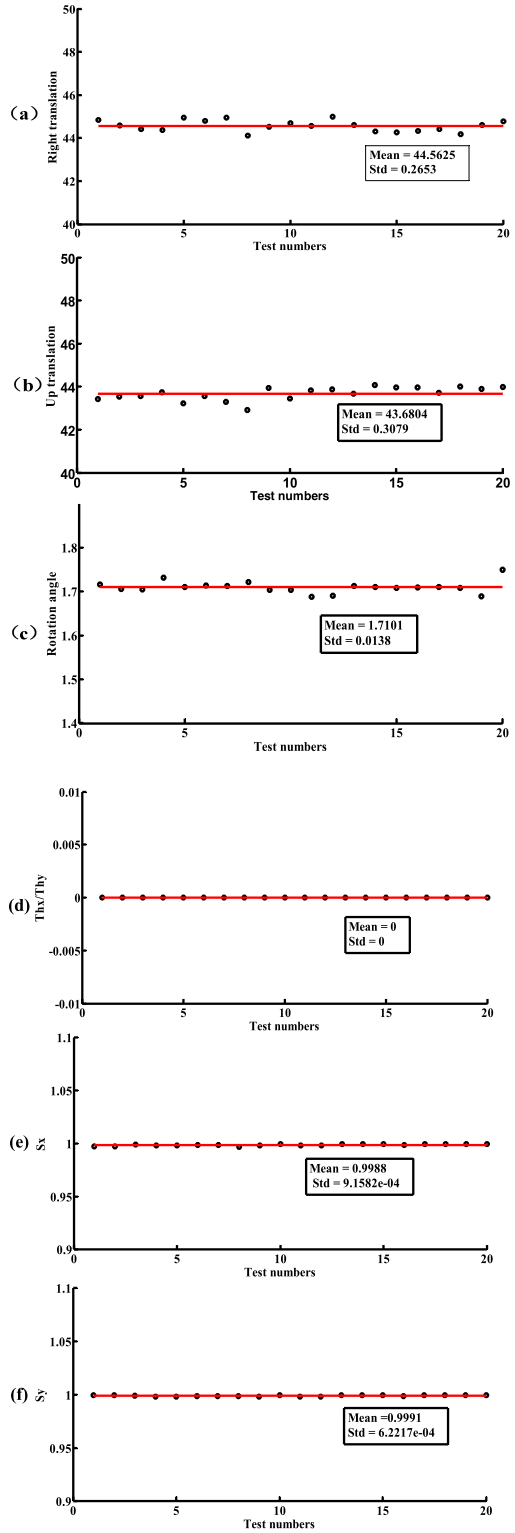

FIGURE 9. Affine transformation matrix parameters for 20 pairs calibration plate images after re-mounting cameras: (a) translation pixels for horizontal direction; (b) translation pixels for vertical direction; (c) rotation angle; (d)tilt angle ThX and ThY for horizontal and vertical direction; (e) zoom factor for horizontal direction Sx; (f) zoom factor for vertical direction Sy. All parameters were measured under the condition of 570nm image as a benchmark.

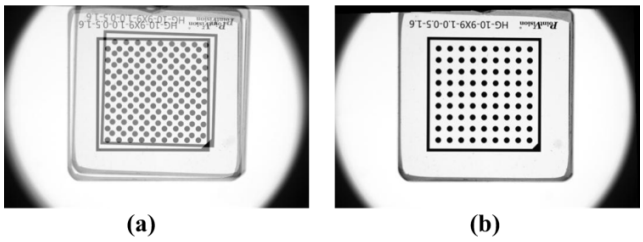

FIGURE 10. The images created by overlaying 570nm and 600nm in the Fig. 3 before and after applying our algorithm, respectively. Misalignment is eliminated in the right image (b) in contrast to the left one (a).

The result showed that the proposed method can successfully register the dual-wavelength images.

B. REGISTRATION RESULTS FOR DUAL-WAVELENGTH RETINAL IMAGES

Using the obtained parameters, misalignment measurements were performed for Fig. 7(a) – Fig. 7(d). The results showed that the proposed method can successfully register the dual-wavelength retinal images, as can be shown in Fig. 11 - Fig. 14. The checkerboard images are used for qualitative comparison.

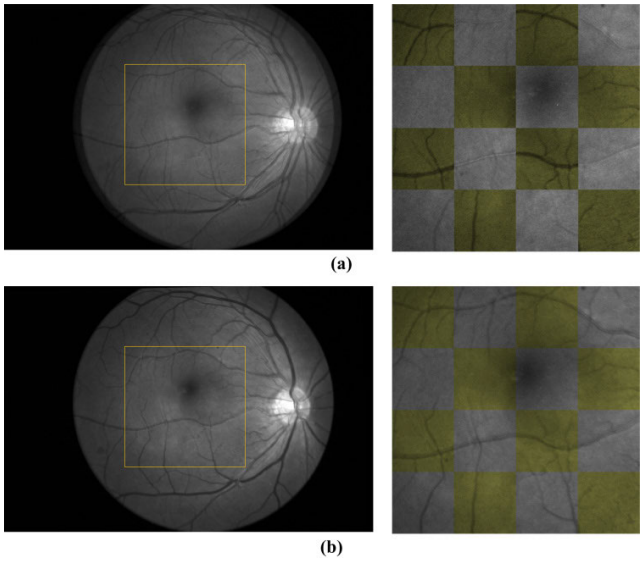

FIGURE 11. Significant misalignment exists between dual-wavelength retinal images and our registration method can handle it effectively. (a) and (b) are the images created by overlaying 570 nm and 600 nm images in Fig. 7(a) before and after applying our method, respectively. Misalignment is eliminated in the bottom image in contrast to the top one. The orange boxes indicate which part of the images are shown in the checkerboards which are provided for qualitative comparison.

Because registration parameters do not vary from person to person, translation and rotation parameters can only be calibrated once and can be saved to a file. In real measurements, parameters are reloaded to calculate blood oxygen saturation. Even if the camera position changes due to human

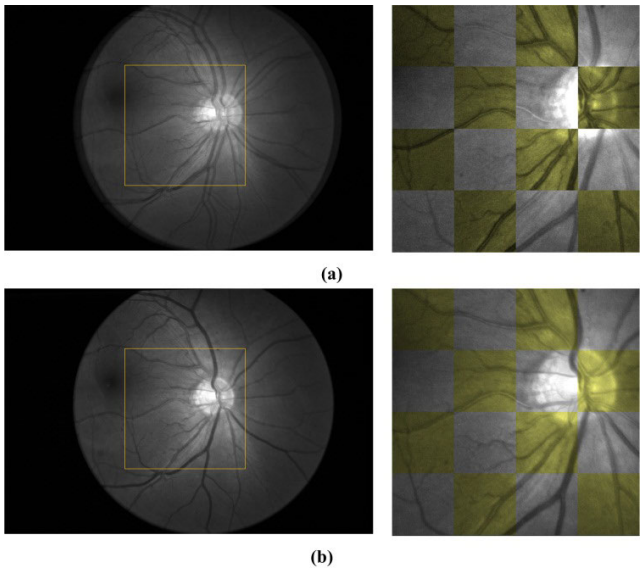

FIGURE 12. Significant misalignment exists between dual-wavelength retinal images and our registration method can handle it effectively. (a) and (b) are the images created by overlaying 570 nm and 600 nm images in Fig. 7(b) before and after applying our method, respectively. Misalignment is eliminated in the bottom image in contrast to the top one. The orange boxes indicate which part of the images are shown in the checkerboards which are provided for qualitative comparison.

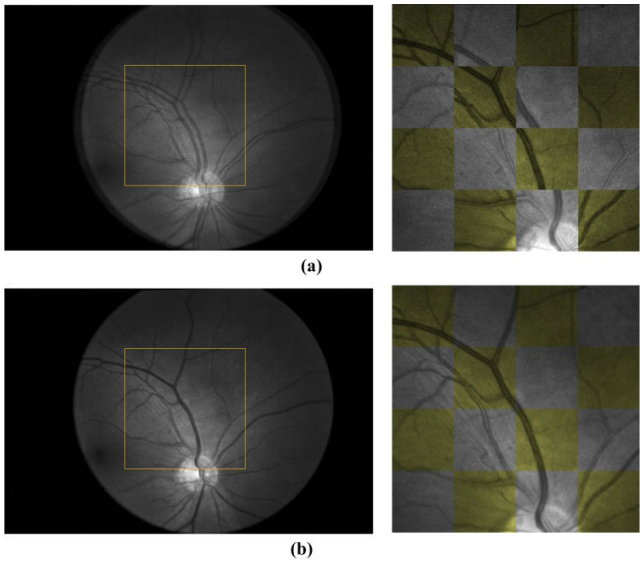

FIGURE 13. Significant misalignment exists between dual-wavelength retinal images and our registration method can handle it effectively. (a) and (b) are the images created by overlaying 570 nm and 600 nm images in Fig. 7(c) before and after applying our method, respectively. Misalignment is eliminated in the bottom image in contrast to the top one. The orange boxes indicate which part of the images are shown in the checkerboards which are provided for qualitative comparison.

factors or external forces, it is only necessary to recollect the dual-wavelength calibration plate images for calibration.

C. EVALUATION

According to above affine transformation matrix parameters analysis, we find that the translation and rotation parameters

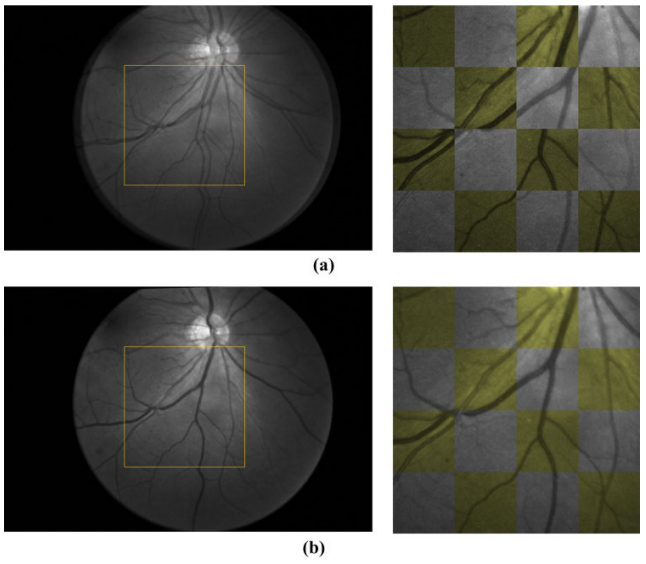

FIGURE 14. Significant misalignment exists between dual-wavelength retinal images and our registration method can handle it effectively. (a) and (b) are the images created by overlaying 570 nm and 600 nm images in Fig. 7(d) before and after applying our method, respectively. Misalignment is eliminated in the bottom image in contrast to the top one. The orange boxes indicate which part of the images are shown in the checkerboards which are provided for qualitative comparison.

between two wavelength images are stable once the CCD cameras were mounted well. It initially proves that the translation and rotation deviation of the dual-wavelength retinal images are caused by the installation deviation of the CCD camera. In order to verify this conclusion, we acquired the dual-wavelength retinal image of 5 volunteers with different fields of view, and proved that the obtained affine transformation matrix parameters can be good for the eliminating misalignment in the dual-wavelength retinal images.

The proposed registration algorithm is evaluated in three aspects, including evaluation of registration errors, evaluation of the effect of registration on calculation of SO_2, and evaluation of running time.

1) EVALUATION OF REGISTRATION ERROR

In order to evaluate the effectiveness of registration, we set 570nm images as a reference image, and use known parameters for translation and rotation to artificially obtain the registered image by image processing software. We compare the registration error of the proposed method to SURF-PIIFD-RPM registration method [7]. We utilized the implementation provided by the authors at https://github.com/gwang-cv/SURF-PIIFD-RPM. It is worth noting that the proposed method is used to analyze the registration error for the calibration plate image. And SURF-PIIFD-RPM is used for retinal image registration. The corresponding translational and rotational parameters are shown in Table 3. The unit of translation transformation is pixel. In the horizontal direction (X direction), positive number represents right translation, and negative number represents left translation. In the vertical

TABLE 3. Results based on image registration.

	Actual transformation parameters			Results for the proposed method		
	X	Y	Angle	X	Y	Angle
1	10	15	5	9.98	15.03	5.001
2	-10	-15	-6	-10.03	-14.97.	-5.998
3	12	-18	7	11.96	-17.96	7.002
4	-15	13	-8	-15.04	12.98	-7.997

TABLE 4. Errors based on the proposed method.

	Actual transformation parameters			Errors for the proposed method/%		
	X	Y	Angle	X	Y	Angle
1	10	15	5	0.20	0.20	0.02
2	-10	-15	-6	0.30	0.20	0.03
3	12	-18	7	0.33	0.22	0.03
4	-15	13	-8	0.27	0.15	0.04

TABLE 5. Results based on SURF-PIIFD-RPM.

	Actual transformation parameters			Results for SURF-PIIFD-RPM		
	X	Y	Angle	X	Y	Angle
1	10	15	5	9.85	15.17	5.08
2	-10	-15	-6	-10.14	-14.81.	-5.89
3	12	-18	7	12.13	-18.21	7.12
4	-15	13	-8	-14.85	13.19	-8.14

TABLE 6. Errors based on SURF-PIIFD-RPM.

	Actual transformation parameters			Errors for SURF-PIIFD-RPM/%		
	X	Y	Angle	X	Y	Angle
1	10	15	5	1.50	1.13	1.60
2	-10	-15	-6	1.40	1.27	1.83
3	12	-18	7	1.08	1.17	1.71
4	-15	13	-8	1.00	1.46	1.75

direction (Y direction), positive numbers represent downward translation, and negative numbers represent upward translation. The unit of rotational angle is degree, negative numbers are counterclockwise, and positive numbers are clockwise. The registration results and errors for each parameter based on the proposed method can be seen in Table 3 and Table 4, respectively. The registration results and errors for each parameter based on SURF-PIIFD-RPM can be seen in the Table 5 and Table 6, respectively. According to Table 4 and Table 6, the mean and standard deviation of registration error for each parameter can be calculated. Based on the proposed registration method, the mean of the corresponding horizontal translation error, vertical translation error, and rotational angle error is 0.28%, 0.19%, and 0.03%, respectively. The standard deviation of each parameter is 0.06%, 0.03%, and 0.09%, respectively. Based on SURF-PIIFD-RPM, the mean of the corresponding horizontal translation error, vertical translation error, and rotational angle error is 1.25%, 1.26%, and 1.72%, respectively. The standard deviation of each parameter is 0.24%, 0.15%, and 0.10%, respectively. It is shown that the proposed method is superior to the SURF-PIIFD-RPM in terms of accuracy and stability of the algorithm.

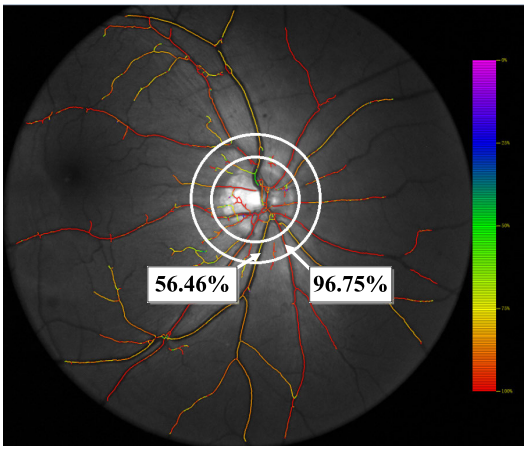

(a)

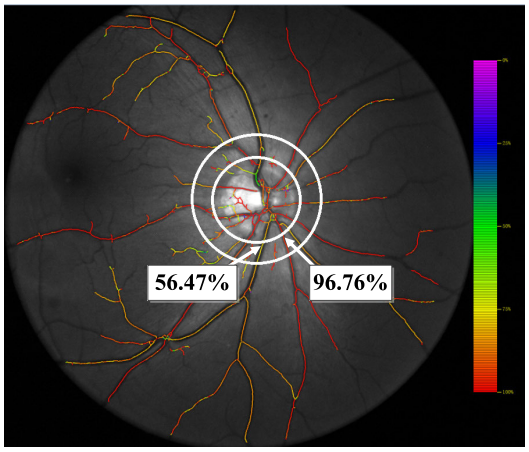

(b)

FIGURE 15. (a)Pseudo color fundus SO_2 map for the retinal images based on the SURF-PIIFD-RPM registration method at the first mounting CCD cameras; (b) Pseudo color fundus SO_2 map for the retinal images based on the proposed registration method at the first mounting CCD cameras.

2) EVALUATION OF THE EFFECT OF REGISTRATION ON CALCULATION OF SO_2

We give two pseudo color fundus SO_2 maps for Fig.1 generated automatically by our SO_2 calculation software, as shown in Fig.15(a) and (b), respectively. They correspond to the results based on SURF-PIIFD-RPM and our proposed registration method, respectively. In order to analyze the how re-mounting CCD cameras effect SO_2, we also give two pseudo color fundus SO_2 maps for the same eye of the individual at the second mounting CCD cameras, as shown in

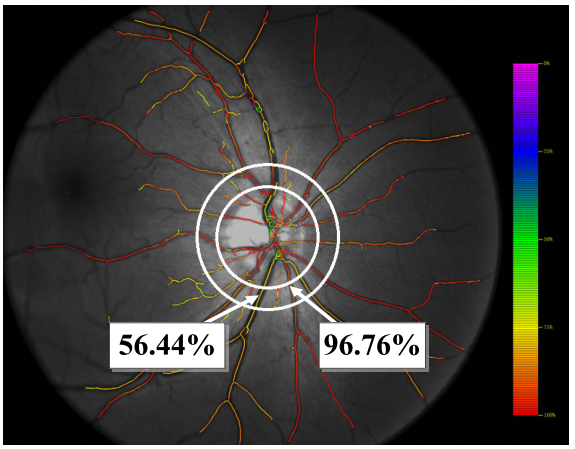

(a)

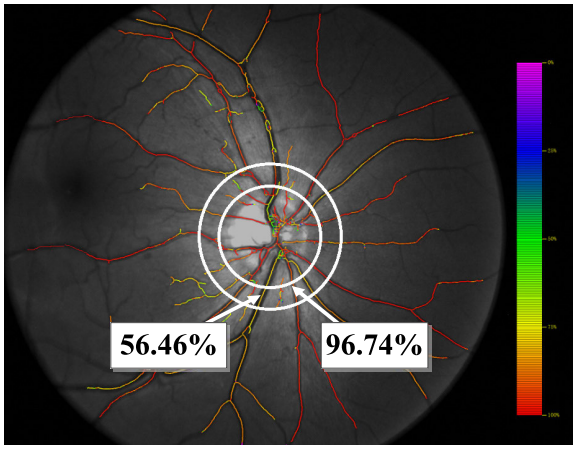

(b)

FIGURE 16. (a)Pseudo color fundus SO_2 map for the same individual based on the SURF-PIIFD-RPM registration method at the second mounting CCD cameras; (b) Pseudo color fundus SO_2 map for the retinal images based on the proposed registration method at the second mounting CCD cameras.

Fig.16(a) and (b), respectively. Colors indicate SO_2 in retinal in retinal vessels (scale to the right of the image). For Fig.15 and Fig.16, two different radius of circles centered on optic disc center were created in order to reduce the influence of optic disc on the calculated SO_2. The SO_2 was determined for corresponding arterial and venous sections in the annular areas. The annular area for blood oxygenation analysis can be determined manually, and our SO_2 calculation software can automatically calculate the SO_2 values for each of the arterial and venous sections. In order to facilitate observation of the results, average SO_2 for one arterial and one venous section in the annular areas are shown in Fig.15 and Fig.16. From the above, we can conclude that compared to SO_2 based on SURF-PIIFD-RPM, the SO_2 values based on the proposed registration method are comparable. There are two main reasons. One is because our SO_2 calculation software employed average SO_2 value of the blood vessel section when calculating SO_2. In addition, both the proposed registration method and SURF-PIIFD-RPM can reach the sub-pixel accuracy and low registration error, so that it will not affect the accuracy of SO_2 calculation.

TABLE 7. The mean and SD of the five images of the same individual based on SURF-PIIFD-RPM at the first mounting CCD cameras.

	Artery	Vein
Mean/%	92.54	56.63
	83.46~101.38	49.94~68.15
SD/%	3.15	3.43
	1.28~5.12	1.18~6.20

For 5 individuals, one artery and one vein were measured in each. Mean and SD were calculated respectively for each individual (from five pairs of images) as a measure of the reproducibility. Table III to Table VI show means and range for these individual means and SDs.

TABLE 8. The mean and SD of the five images of the same individual based on the proposed registration method at the first mounting CCD cameras.

	Artery	Vein
Mean/%	92.56	56.65
	83.45~101.28	49.91~68.15
SD/%	3.14	3.42
	1.27~5.11	1.20~5.98

TABLE 9. The mean and SD of the five images of the same individual based on SURF-PIIFD-RPM at the second mounting CCD cameras.

	Artery	Vein
Mean/%	92.60	56.61
	83.47~101.32	49.86~68.24
SD/%	3.13	3.40
	1.26~5.13	1.17~6.16

A study in the 5 healthy volunteers was performed for evaluating the effect of the proposed registration method on the reproducibility of the retinal oximetry. Five fundus images of each subject under the condition of scenario 2 were recorded. For each of the five images, average SO_2 for one arterial and one venous section in the annular areas are calculated, as shown in Fig.15 and Fig.16. Table 7 shows the mean and SD of the five repeated measurements of the same vessel section based on SURF–PIIFD–RPM at the first mounting CCD cameras. And Table 8 shows the mean and SD of the five repeated measurements of the same vessel section based on the proposed registration method at the first mounting CCD cameras. And Table 9 shows the mean and SD of the five repeated measurements of the same vessel section based on SURF–PIIFD–RPM at the second mounting CCD cameras. Table 10 shows the mean and SD of the five repeated measurements of the same vessel section based on the proposed registration method at the second mounting CCD cameras. According to Table 7 - Table 10, SO_2 values have comparable accuracy under the four conditions. This phenomenon agrees well with the theoretical analysis. It also proves the applicability of our registration method.

TABLE 10. The mean and SD of the five images of the same individual based on the proposed registration method at the second mounting CCD cameras.

	Artery	Vein
Mean/%	92.59	56.60
	83.44~101.26	49.85~68.19
SD/%	3.12	3.35
	1.26~5.19	1.19~6.08

3) EVALUATION OF RUNNING TIME

After testing, under the same hardware conditions(CPU: Intel(R) Core(TM) i5-4200U, Frequency: 1.60 GHZ, Memory: 4G), means and standard deviations(std) of runtime for all outputs of our proposed method and SURF–PIIFD–RPM are 0.36±0.19ms, 30.27±7.48s, respectively. It can be seen that our proposed method is much more computationally efficient than SURF–PIIFD–RPM. It can greatly save the entire time for SO_2 calculation procedure.

Based on the above analysis, the SO_2 values based on the two registration methods are well-matched. And the proposed registration method can significantly improve SO_2 calculation speed while ensuring accuracy. Because registration parameters do not vary from person to person, translation and rotation parameters can only be calibrated once and can be saved to a file. Before SO_2 measurements, parameters are reloaded to realize the dual-wavelength retinal images. Even if the camera position changes due to human factors or external forces, it is necessary and convenient to re-acquire the dual-wavelength calibration plate images for calibration and obtain the affine transformation matrix parameters.

V. DISCUSSIONS

In this paper, we proposed a registration method based on camera calibration for aligning dual-wavelength retinal images. Since the intensity of the images is substantially different, the registration needs to rely only on the structural features that the image pairs have in common. Whereas previously many proposed existing registration approaches include a vessel segmentation step or point matches for dual-wavelength retinal images as part of their algorithms, the errors in vessel segmentation or point matches could potentially propagate into the registration process as well. In this work, we employed feature extraction and affine transformation matrix calculation to capture the known structural information of standard calibration plate in the images so as not to require the segmentation of blood vessels or point matches for dual-wavelength retinal images. Once the 20 pairs of dual-wavelength images for calibration plate were acquired, our proposed method only needs on average less than 4 milliseconds to perform the registration which is considerably fast. Hence, removing the vessel segmentation step reduces the required time for registering the dual-wavelength retinal images.

Furthermore, the proposed method is capable of registering the dual-wavelength retinal images acquired from unhealthy eyes. This is because the proposed registration method does not directly use the character of dual-wavelength retinal images. It makes registering the pathological retinal images less challenging. However, our work was based on healthy retinal images. The potential limitation is that we have not looked at pathological images. As in diseases, there may be lesions which may alter the pixels in the box. A pilot on pathological images would add value. Besides, there are only 5 healthy volunteers in this study, some differences may not show statistical laws, so we need a lot of further detailed research and analysis, including test-retest variability. Ongoing work is required to strengthen cooperation with hospitals and acquire more healthy and pathological retinal images for further analysis. The pathological changes may be caused by diabetic retinopathy, glaucoma, vascular occlusion and so on.

In addition, our work was based on well-defined assumption that retinal shape was planar. However it has been shown that spherical or even ellipsoidal shape estimation can further improve registration results [16]. Ongoing work is required to take into account the retinal shape further improve the results obtained.

Even though the view field of rectangular box for the standard calibration plate is much less than that of retinal images, the registration parameters were suitable for registering the dual-wavelength retinal images in our system, due to the fact that 20 typical experimental conditions totally include corresponding view field of retinal images and therefore, significant information has been added for aligning image pairs. The parameters calculated by 20 pairs typical calibration images are basically stable. The experimental results can also indicate the above conclusion.

The experimental results show that the translation and rotation parameters are only related to the CCD camera installation of the system itself. We also show that the parameters obtained can be robust for the registration of dual-wavelength retinal images. And we also proved re-mounting CCD cameras did not affect SO_2 values. This work has important practical value and engineering significance, which lays the foundation for the clinical application of retinal oximetry.

VI. CONCLUSION

According to analysis in section II, there only exists the translation and rotation deviation between the dual-wavelength retinal images caused by a mounting deviation of CCD cameras in the retinal oximetry. It needs image registration before SO_2 calculation. Therefore, we propose a robust registration based on camera calibration that is capable of aligning 570nm and 600nm modalities without requiring dual-wavelength retinal images with the aim of reducing the registration error and speeding up the registration process. The proposed method does not depend on the dual-wavelength retinal images, and can avoid registration error caused by retinal image quality, for example, vessel segmentation or point matches may lead to error in the diabetic retinopathy images.

Experiments with calibration plate images demonstrate that the translation and rotation parameters do not change with external conditions, and they are related to the system itself. To the best of our knowledge, this is the first time to improve the registration accuracy and speed in retinal oximetry through reason analysis for the misalignment between dual-wavelength images, and using camera calibration to realize registration. We also demonstrate the obtained parameters can robustly registering the real dual-wavelength retinal images from a series of 5 healthy subjects.

For every retinal oximetry, once the rotation and translation parameters were determined, they can be written into the retinal oxygen saturation calculation software. The misalignment can be automatically proposed after inputting the dual-wavelength retinal image. And the aligned images can be directly employed in subsequent image processing and SO_2 calculation. Hence, it greatly reduces the time of registration. Simplifying the retinal images registration step is beneficial as it prevents propagating the possible registration errors to the registration process, especially under the condition of pathological retinal images. It can provide much more reliable SO_2 values whether the human eye is healthy or not. Results for healthy retinal images demonstrated that the proposed registration method can significantly improve SO_2 calculation speed while ensuring accuracy. It is much more convenient and efficient for doctors who operate retinal oximetry.

ACKNOWLEDGMENT

The authors would like to thank the anonymous reviewers and the Associate Editor for providing constructive and generous feedback.

REFERENCES

[1] A. Harris, R. B. Dinn, L. Kagemann, and E. Rechtman, "A review of methods for human retinal oximetry," *Ophthalmic Surg. Lasers Imag.*, vol. 34, no. 2, pp. 152–164, Mar./Apr. 2003.

[2] O. B. Olafsdottir, S. H. Hardarson, M. S. Gottfredsdottir, A. Harris, E. Stefánsson, "Retinal oximetry in primary Open-Angle glaucoma," *Investigative Ophthalmol. Vis. Sci.*, vol. 52, no. 9, pp. 6409–6413, Aug. 2011.

[3] S. H. Hardarson and E. Stefánsson, "Retinal oxygen saturation is altered in diabetic retinopathy," *Brit. J. Ophthalmol.*, vol. 96, no. 4, pp. 560–563, Mar. 2012.

[4] S. H. Hardarson, S. Basit, T. E. Jonsdottir, T. Eysteinsson, G. H. Halldorsson, R. A. Karlsson, J. M. Beach, J. A. Benediktsson, and E. Stefansson, "Oxygen saturation in human retinal vessels is higher in dark than in light," *Investigative Ophthalmol. Vis. Sci.*, vol. 50, no. 5, pp. 2308–2311, May 2009.

[5] J. Beach, "Pathway to retinal oximetry," *Transl. Vis. Sci Technol.*, vol. 3, no. 5, p. 2, Sep. 2014.

[6] M. D. Abràmoff, M. K. Garvin, and M. Sonka, "Retinal imaging and image analysis," *IEEE Rev. Biomed. Eng.*, vol. 3, pp. 169–208, 2010.

[7] G. Wang, Z. Wang, Y. Chen, and W. Zhao, "Robust point matching method for multimodal retinal image registration," *Biomed. Signal Process. Control*, vol. 19, pp. 68–76, Apr. 2015.

[8] S. K. Saha, D. Xiao, A. Bhuiyan, T. Y. Wong, and Y. Kanagasingam, "Color fundus image registration techniques and applications for automated analysis of diabetic retinopathy progression: A review," *Biomed. Signal Process. Control*, vol. 47, pp. 288–302, Jan. 2019.

[9] S. K. Saha, D. Xiao, S. Frost, and Y. Kanagasingam, "A two-step approach for longitudinal registration of retinal images," *J. Med. Syst.*, vol. 40, no. 12, p. 277, Dec. 2016.

[10] R. Gomathy, L. Marco, and D. Nicholas, "Registration of adaptive optics corrected retinal nerve fiber layer (RNFL) images," *Biomed. Opt. Express*, vol. 5, no. 6, pp. 1941–1951, May 2014.

[11] J. Lezama, D. Mukherjee, R. P. McNabb, G. Sapiro, A. N. Kuo, and S. Farsiu, "Segmentation guided registration of wide field-of-view retinal optical coherence tomography volumes," *Biomed. Optics Express*, vol. 7, no. 12, pp. 4827–4846, Dec. 2016.

[12] Z. Chen, L. Zhang, and G. Zhang, "An improved InSAR image co-registration method for pairs with relatively big distortions or large incoherent areas," *Sensors*, vol. 16, no. 9, p. 1519, Sep. 2016.

[13] H. G. Halldorsson, J. A. Benediktson, G. M. Zoega, T. Eysteinsson, and E. Stefansson, "Automatic registration of spectrophotometric retinal images," in *Proc. 6th Nordic Signal Process. Symp.-(NORSIG)*, 2004, pp. 5–8.

[14] X. Yongli, D. Yun, and G. Chunming, "Dual-wavelength retinal image registration based on vessel segmentation and optic disc detection," *Proc. SPIE*, vol. 9684, Sep. 2016, Art. no. 986417.

[15] J. Lin, Y. Zheng, W. Jiao, B. Zhao, S. Zhang, J. Gee, and R. Xiao, "Group-wise registration of sequential images from multispectral imaging(MSI) of the retina and choroid," *Opt. Express*, vol. 24, no. 22, pp. 25277–25290, Oct. 2016.

[16] C. Hernandez-Matas, X. Zabulis, A. Triantafyllou, P. Anyfanti, and A. A. Argyros, "Retinal image registration under the assumption of a spherical eye," *Computerized Med. Imag. Graph.*, vol. 55, pp. 95–105, Jan. 2017.

[17] L. Zhang, B. Li, L. Tian, and W. Zhu, "LPPCO: A novel multimodal medical image registration using new feature descriptor based on the local phase and phase congruency of different orientations," *IEEE Access*, vol. 6, pp. 71976–71987, 2018.

[18] G. Lv, "Self-similarity and symmetry with SIFT for multi-modal image registration," *IEEE Access*, vol. 7, pp. 52202–52213, 2019.

[19] M. S. Miri, M. D. Abrámoff, Y. H. Kwon, and M. K. Garvin, "Multi-modal registration of SD-OCT volumes and fundus photographs using histograms of oriented gradients," *Biomed. Opt. Express*, vol. 7, no. 12, pp. 5252–5267, Dec. 2016.

[20] H. M. Taha, N. El-Bendary, A. E. Hassanien, Y. Badr, and V. Snase, "Retinal feature-based registration schema," in *Proc. Inform. Eng. Inf. Sci.* Boston, MA, USA: Springer, 2011, pp. 26–36.

[21] K. Deng, J. Tian, J. Zheng, X. Zhang, X. Dai, and M. Xu, "Retinal fundus image registration via vascular structure graph matching," *Int. J. Biomed. Imag.*, vol. 2010, Jul. 2010, Art. no. 906067.

[22] T. Che, Y. Zheng, J. Cong, Y. Jiang, Y. Niu, W. Jiao, B. Zhao, and Y. Ding, "Deep group-wise registration for multi-spectral images from fundus images," *IEEE Access*, vol. 7, pp. 27650–27661, 2019.

[23] R. Liao, S. Miao, P. de Tournemire, S. Grbic, A. Kamen, T. Mansi, and D. Comaniciu, "An artificial agent for robust image registration," in *Proc. 31st AAAI Conf. Artif. Intell.*, Feb. 2016, pp. 1–8.

[24] M. Polfliet, S. Klein, W. Huizinga, M. M. Paulides, W. J. Niessen, and J. Vandemeulebroucke, "Intrasubject multimodal groupwise registration with the conditional template entropy," *Med. Image Anal.*, vol. 46, pp. 15–25, May 2018.

[25] Ž. Špiclin, B. Likar, and F. Pernuš, "Groupwise registration of multimodal images by an efficient joint entropy minimization scheme," *IEEE Trans. Image Process.*, vol. 21, no. 5, pp. 2546–2558, May 2012.

[26] Y. Zheng, Y. Wang, W. Jiao, S. Hou, Y. Ren, M. Qin, D. Hou, C. Luo, H. Wang, J. Gee, and B. Zhao, "Joint alignment of multispectral images via semidefinite programming," *Biomed. Opt. Express*, vol. 8, no. 2, pp. 890–901, Feb. 2017.

[27] Y. Xian, Y. Dai, C. Gao, and R. Du, "Dual-wavelength retinal images denoising algorithm for improving the accuracy of oxygen saturation calculation," *Proc. SPIE*, vol. 22, no. 1, Jan. 2017, Art. no. 016004.

[28] *HALCON—The Power of Machine Vision*. Accessed: 2018. [Online]. Available: http://www.mvtec.com/products/halcon

[29] L. Li, "Research on multi-view vision measurement method based on halcon," M.S. thesis, Shenyang Aerosp. Univ., Liaoning, China, 2014.

[30] S. Zhang, B. Li, F. Ren, and R. Dong, "High-precision measurement of binocular telecentric vision system with novel calibration and matching methods," *IEEE Access*, vol. 7, pp. 54682–54692, Apr. 2019.

YONG-LI XIAN received the Ph.D. degree from the School of Optoelectronic Science and Engineering, University of Electronic Science and Technology of China. She is currently a Lecturer with the School of Electrical Engineering and Electronic Information, Xihua University. Her current research interests include biomedical optics, biomedical imaging processing, and biomedical information processing.

CONG-ZHENG WANG received the Ph.D. degree from the School of Optoelectronic Science and Engineering, University of Electronic Science and Technology of China. He is currently an Associate Professor Fellow with the Institute of Optics and Electronics, Chinese Academy of Sciences. His current research interests include special photoelectric detection, photoelectric treatment, and photoelectric measurement.

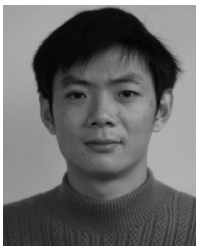

YUN DAI received the Ph.D. degree from the Institute of Optics and Electronics, Chinese Academy of Sciences, where he is currently a Professor Fellow. His current research interests include biomedical optics, biomedical optical instruments, and adaptive optics.